Journal of Materials Chemistry A



PAPER View Article Online
View Journal | View Issue



Cite this: *J. Mater. Chem. A*, 2018, 6, 11743

of thermoelectric CuInTe₂ through quantum mechanics†

Determining ideal strength and failure mechanism

Guodong Li, 60 *ab Qi An, 60 c Sergey I. Morozov, 60 d Bo Duan, a Pengcheng Zhai, a Qingjie Zhang, *a William A. Goddard III and G. Jeffrey Snyder 60 b

CuInTe₂ is recognized as a promising thermoelectric material in the moderate temperature range, but its mechanical properties important for engineering applications remain unexplored so far. Herein, we applied quantum mechanics (QM) to investigate such intrinsic mechanical properties such as ideal strength and failure mechanism along with pure shear, uniaxial tension, and biaxial shear deformations. We found that the ideal shear strength of CuInTe₂ is 2.43 GPa along the (221)[11–1] slip system, which is much lower than its ideal tensile strength of 4.88 GPa along [1–10] in tension, suggesting that slipping along (221)[11–1] is the most likely activated failure mode under pressure. Shear induced failure of CuInTe₂ arises from softening and breakage of the covalent In–Te bond. However, tensile failure arises from breakage of the Cu–Te bond. Under biaxial shear load, compression leads to shrinking of the In–Te bond and consequent buckling of the In–Te hexagonal framework. We also found that the ideal strength of CuInTe₂ is relatively low among important thermoelectric materials, indicating that it is necessary to enhance the mechanical properties for commercial applications of CuInTe₂.

Received 25th April 2018 Accepted 24th May 2018

DOI: 10.1039/c8ta03837f

rsc.li/materials-a

1. Introduction

Since the 20th century, rapid industrialization has led to overconsumption of fossil fuels, causing severe environmental concerns such as global warming, acid rain, and air pollution. The search for alternative eco-friendly energy technology has attracted worldwide attention. Thermoelectrics (TEs), which directly convert heat into electrical energy without causing environmental pollution, could play an essential role in relieving the global energy crisis. ^{1,2} An excellent TE material should simultaneously possess robust mechanical behavior and high material performance, which is characterized by the figure of merit, $zT = \alpha^2 \sigma T/\kappa$, where α is the Seebeck coefficient, σ is the

Recently, a ternary I-III-VI2 compound CuInTe2 was reported as a promising p-type TE semiconductor with zT value larger than 1 at \sim 850 K.8 CuInTe₂ has a direct bandgap of 1.02 eV with multiple degenerate bands near the valence band maximum,9 which leads to a high Seebeck coefficient. In addition, its intrinsic thermal conductivity is \sim 6 W m⁻¹ K⁻¹ at room temperature, 10 which is much higher than other important TE materials such as Mg-Si-Sn alloys (~2 W m⁻¹ K⁻¹)¹¹ and filled skutterudites (~2 W m⁻¹ K⁻¹). Thus, many approaches have been developed to increase electrical conductivity and reduce thermal conductivity to enhance the zT values of CuInTe₂. ¹³⁻¹⁶ For example, embedding graphene sheets into the CuInTe₂ matrix strengthens the interface phonon scattering, decreasing thermal conductivity and hence improving the zT value.13 Substitution of Cd at the In site $(CuIn_{1-x}Cd_xTe_2)$ can effectively increase carrier concentration, leading to sharp enhancement of electrical conductivity.10 Similarly, Sb substitution at the Te

electrical conductivity, κ is the thermal conductivity, and T is the temperature. In the past decade, various strategies have been developed to enhance the zT values of TE materials, $^{3-6}$ but research on mechanical properties is lagging, which limits the industrial applications of TE materials. Under thermal cycling conditions of TE devices, thermomechanical stresses easily cause cracks or fatigue damage in TE materials, 7 accelerating deterioration of material performance as well as failure of TE devices. Thus, improving mechanical properties such as mechanical strength and toughness is significant for development of reliable TE devices.

[&]quot;State Key Laboratory of Advanced Technology for Materials Synthesis and Processing, Wuhan University of Technology, Wuhan 430070, China. E-mail: guodonglee@whut. edu.cn; zhangqj@whut.edu.cn

^bDepartment of Materials Science and Engineering, Northwestern University, Evanston, Illinois 60208. USA

Department of Chemical and Materials Engineering, University of Nevada Reno, Reno, Nevada 89557. USA

^dDepartment of Computer Simulation and Nanotechnology, South Ural State University, Chelyabinsk 454080, Russia

^eMaterials and Process Simulation Center, California Institute of Technology, Pasadena, California 91125. USA

[†] Electronic supplementary information (ESI) available: Explanation of how we compute stress-strain relations; ELF change for CuInTe₂ under (221)[11–1] pure shear load, [1–10] tension load, and (221)[11–1] biaxial load. See DOI: 10.1039/c8ta03837f

site (CuInTe $_{2-x}$ Sb $_x$) leads to drastic improvement in power factor (1445 μ W m $^{-1}$ K $^{-2}$) owing to simultaneous enhancement of electrical conductivity and Seebeck coefficient. In addition, introduction of In $_2$ O $_3$ nanoinclusions into this sample can further reduce thermal conductivity. Thus, a record high zT value of 1.61 at \sim 850 K was achieved for the CuInTe $_2$ TE material. However, its mechanical properties, which are important for reliability of CuInTe $_2$ -based TE devices, remain unexplored so far.

To determine the intrinsic mechanical properties, such as ideal strength and deformation mechanism of CuInTe₂, we applied quantum mechanics (QM) based density functional theory (DFT) at the Perdew–Burke–Ernzerhof (PBE) functional level to investigate the responses against pure shear, uniaxial tension, and bi-shear deformations. We first determined the most plausible slip and tensile systems. Then, we characterized in detail the stress–strain relationship, ideal strength and failure modes under various loading conditions. Finally, fracture toughness was computed based on the stress–strain relationship. Discussions are presented regarding the comparison of CuInTe₂ with other important TE materials.

Among all the shear paths, (221)[11–1] was found to have the lowest ideal shear strength of 2.43 GPa, and the softening and breakage of the In–Te bond was responsible for shear failure of CuInTe₂. Moreover, under the [1–10] tension load, CuInTe₂ was found to have the lowest tensile strength of 4.88 GPa, and the Cu–Te bond dominates the deformation and tensile failure of CuInTe₂. Under biaxial shear deformation, the maximum shear stress was 1.95 GPa, which was much lower than that under pure shear deformation. Failure arises from compression of In–Te bond and buckling of the 3D In–Te hexagonal framework. These mechanical strengths and structural deformation modes demonstrate intrinsic structure–mechanical property relations, which are helpful for the development of mechanically robust and reliable CuInTe₂ TE devices.

2. Methodology

Ideal strength and deformation mechanism calculations were performed using the VASP code, utilizing projector augmented wave (PAW) potentials. 17-19 Exchange-correlation functional was calculated within the Perdew-Burke-Ernzerhof (PBE) level to account for core-valence interactions.20 Valence electrons for Cu, In, and Te were set as 3d¹⁰4s¹, $5s^25p^1$, and $5s^25p^4$, respectively. Herein, we applied PBE + U method (U = 4 eV) to describe the exchange-correlation efforts of the Cu 3d electrons.9 A 500 eV plane-wave energy cutoff was adopted for convergence on force and geometries. Energy errors for terminating electronic self-consistent field (SCF) and force criterion convergence were set to 1×10^{-6} eV and 1×10^{-2} eV Å^{-1} , respectively. Monkhorst-Pack grid with fine resolution of $2\pi \times 1/40 \text{ Å}^{-1}$ was used for all calculations. The pure shear, uniaxial tension, and bi-shear simulations are similar to our previous studies on other important TE materials,21-23 as explained in the ESI†.

Results and discussion

3.1 Crystal structure and chemical bonding

CuInTe₂ crystallizes in tetragonal structure (space group I42d), which originates from diamond-like cubic zinc-blende material, as shown in Fig. 1(a). The unit cell contains 16 atoms ($4 \times Cu$, 4 \times In, and 8 \times Te); each Cu or In atom is tetrahedrally coordinated with Te. The structure consists of a 3D framework linked by Cu-Te (2.62 Å) and In-Te (2.86 Å) bonds. As shown in Fig. 1(b), the calculated electron localized function (ELF), which can be used to analyze bonding character,24 clearly shows shared electrons between In3+ and Te2-, suggesting covalent bonding character of In-Te with a Pauling electronegativity (EN) difference of 0.32 ($\chi_{\rm In} = 1.78$, $\chi_{\rm Te} = 2.10$). The EN difference for Cu-Te is 0.2 ($\chi_{Cu}=1.90,\,\chi_{Te}=2.10$), which is much smaller than that of In-Te (0.32). This suggests stronger covalent bonding interaction in Cu-Te than In-Te. The DFT optimized lattice parameters are a = 6.30 and c = 12.67 Å, which are only 1.6% and 1.9% larger than the experimental values of a = 6.20and c = 12.43 Å at room temperature, ²⁵ and show good agreement with previous theoretical values of a = 6.29 and c = 12.60Å from PBE functional.26

3.2 Ideal strength, deformation and failure mechanism

3.2.1 Pure shear deformation of CuInTe₂. Ideal strength, deformation and failure mechanism of a crystal are intrinsic mechanical behaviors closely related to the nature of chemical bonds,²⁷ and the failure mode depends on the type of applied stress, such as shear, tension or compression. Herein, we applied pure shear and uniaxial tension loads to explore theoretical strength and deformation mechanism of CuInTe₂.

To understand ideal shear strength of CuInTe₂, we examined the pure shear stress response against shear strain along different slip systems. The computed shear-stress–shear-strain relationships for CuInTe₂ are shown in Fig. 2(a). The (221) [11–1] slip system was found to have the ideal shear strength (maximum stress point) of 2.43 GPa, which is lower than those shearing along the (221)[1–10] (2.57 GPa), (001)[1–10] (5.54 GPa), (001)[100] (4.98 GPa), and (010)[100] (5.35 GPa) systems. This indicates that the (221)[11–1] slip system is the most likely

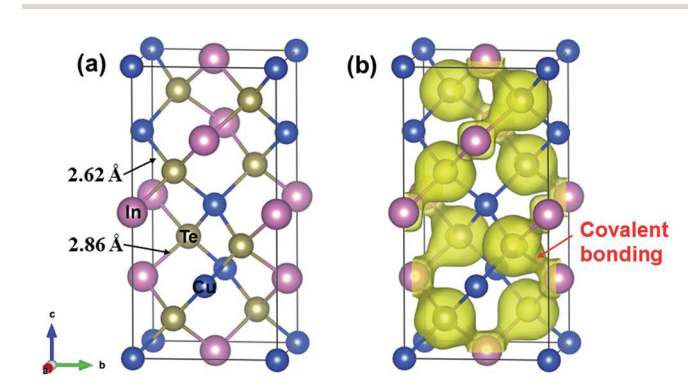


Fig. 1 (a) Crystal structure and (b) chemical bonding (with calculated isosurfaces at a value of 0.75 of ELF) of ternary $I-III-VI_2$ compound $CuInTe_2$.

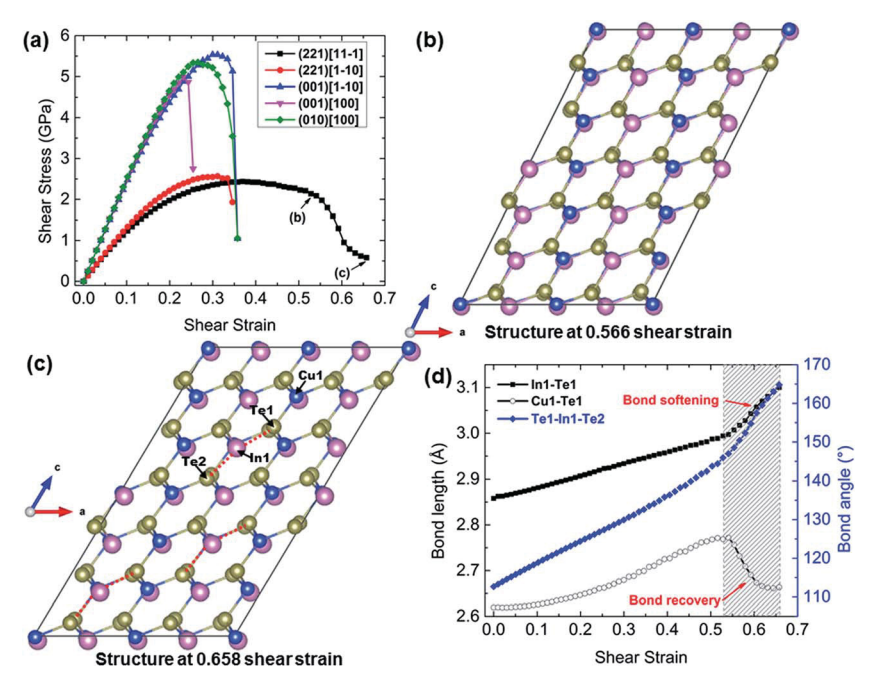


Fig. 2 Pure shear deformation and failure mechanism of $CuInTe_2$. (a) Shear-stress—shear-strain relationships for $CuInTe_2$ along different slip systems. The atomic structures of $CuInTe_2$ shearing along the least stress slip system of (221)[11–1]: (b) atomic structure at 0.566 shear strain and (c) atomic structure at 0.658 shear strain corresponding to the highly softened structure. (d) Typical bond lengths (In1–Te1 and Cu1–Te1) and bond angle (Te1–In1–Te2) against shear strain along the (221)[11–1] slip system. The gray dashed region corresponds to the structural softening stage.

cleavage system for $CuInTe_2$ under pressure. Beyond the maximum stress point, the shear stress in the (221)[11-1] system gradually decreases until structural failure, suggesting a significant 'yielding' and structural softening process, while the shear stress in other slip systems shows a sudden drop, suggesting typical brittle failure and structural collapse processes.

To explain this 'yielding' process in the least stress slip system and determine the shear failure mechanism of CuInTe₂, we extracted the structure patterns and typical bond lengths (angles) to investigate the bond-responding process along the (221)[11-1] slip system, as shown in Fig. 2(b)-(d). As shear strain increases to 0.566, the In-Te and Cu-Te hexagonal frameworks, consisting of both In-Te and Cu-Te bonds, distort to resist shear deformation (Fig. 2(b)). The In1-Te1 bond is linearly stretched from 2.86 to 3.02 Å with stretching ratio of 5.6%, while Te1-In1-Te2 bond angle linearly increases from 112.7° to 150.4° , accommodating shear deformation. Moreover, the Cu1-Te1 bond is stretched from 2.62 to 2.73 Å with smaller stretching ratio of 4.2%. When shear strain further increases to 0.658, corresponding to the highly softened structure (Fig. 2(c)), the In-Te bonds break, representing collapse of the In-Te hexagonal framework. However, Cu-Te bonds are still connected, maintaining the integrity of the In-Te hexagonal framework. This explains why shear stress decreases to 0.58 GPa, rather than zero, at 0.658 shear strain. During this structural softening process (Fig. 2(d)), the In1-Te1 bond is rapidly stretched to 3.1 Å, leading to the sharply increased Te1-In1-Te2 bond angle. This highly softened or non-bonding In-Te

interaction is responsible for structural stiffness softening (Fig. 2(c)) and rapidly reduces shear stress (Fig. 2(a)). Softening of the In–Te bond dominates the 'yielding' deformation along the (221)[11-1] system. This explains why there is no sudden drop in shear stress, as shown in Fig. 2(a). The Cu1–Te1 bond rapidly shrinks to 2.66 Å, representing significant bond recovery, which suppresses structural softening.

We also extracted ELF change against shear strain to further understand the bond-responding process along (221)[11–1] system, as shown in Fig. S2 in ESI.† As shear strain increases to 0.566 before structural softening, the In–Te bonds still possess shared electrons, suggesting no bond breakage. However, at 0.658 shear strain, which corresponds to the highly softened structure, the shared electrons between In–Te move completely towards individual In and Te atoms, suggesting breakage of the In–Te bond. ELF change between In–Te further confirms that softening and breakage of the In–Te bonds leads to structural softening and shear failure of CuInTe₂.

3.2.2 Uniaxial tensile deformation of CuInTe₂. To understand ideal tensile strength and deformation mechanism of CuInTe₂, we imposed uniaxial tensile loading along different tensile systems to examine structure-mechanical property relations. Fig. 3(a) displays the calculated tensile-stress-tensile-strain relations. In all the tensile systems, with an increase in tensile strain, the tensile stress rapidly increases until maximum tensile stress is achieved, indicating the structure strongly resists tensile deformation. Beyond this point, the tensile stress suddenly drops, indicating structural collapse and brittle failure. Among these tensile systems, the system under

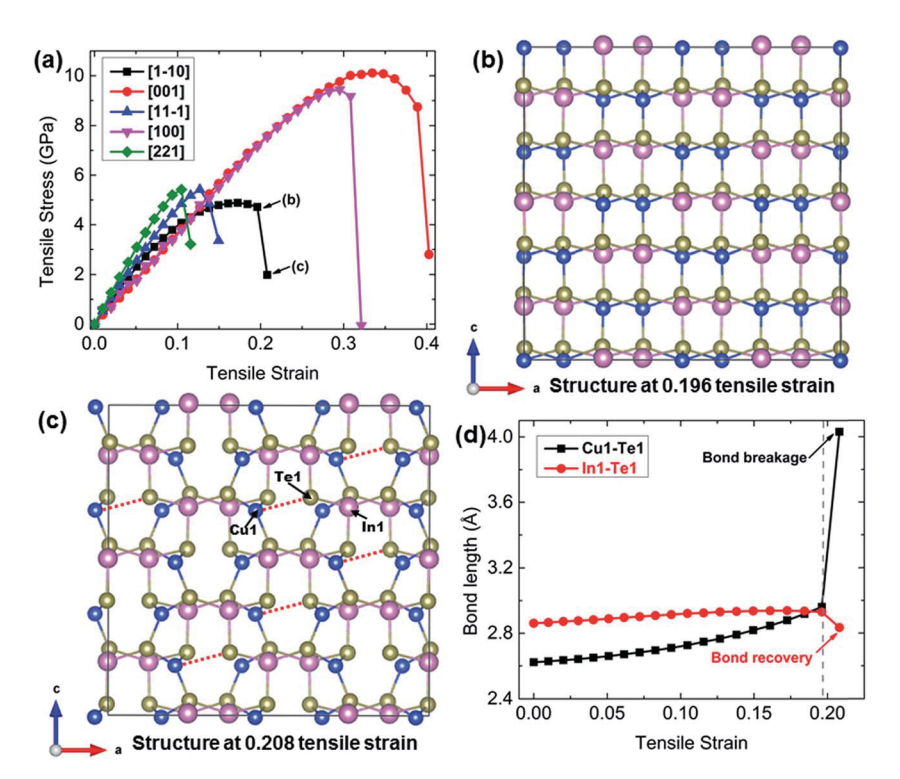


Fig. 3 Uniaxial tension deformation and failure mechanism of $CuInTe_2$. (a) Tensile-stress—tensile-strain relationships for $CuInTe_2$ under different tension loads. The atomic structures of $CuInTe_2$ tension along least tensile-stress system of [1–10]: (b) atomic structure at 0.196 tensile strain before failure and (c) atomic structure at failure strain of 0.208. (d) Typical bond lengths (Cu1-Te1 and In1-Te1) as a function of tensile strain along the [1–10] tension system. The gray dashed line represents tensile strain before failure.

[1-10] tension load was found to have the lowest ideal tensile strength of 4.88 GPa at 0.173 tensile strain. This ideal tensile strength is much higher than the ideal shear strength of 2.43 GPa, indicating that shear failure is much easier to occur than tensile failure for CuInTe2. Fig. 3(b) and (c) show the structural patterns before and at failure strains, respectively. At 0.196 tensile strain before failure, the structure can still hold together with perfect structural integrity (Fig. 3(b)). At failure strain of 0.208, the Cu1-Te1 bond breaks, leading to sudden drop of tensile stress (Fig. 3(a)) and structural failure. However, the In1-Te1 bond is still connected, indicating that the structure is not totally cleaved along the [1-10] plane. Before failure, the Cu1-Te1 bond is stretched from 2.62 to 2.96 Å with a stretching ratio of 13.0%, while the In1-Te1 bond is slightly stretched with a stretching ratio of 2.4%, as shown in Fig. 3(d). This implies that the Cu1-Te1 bond is less rigid than the In1-Te1 bond, suggesting that the Cu1-Te1 bond softens before In1-Te1 bond breaks. Thus, Cu1-Te1 bond breaks at a failure strain of 0.208, releasing structural stress. Moreover, the In1-Te1 bond length recovers to 2.84 Å. The stretching force constant (SFC) calculation using ATAT code²⁸ shows that the SFC of the Cu–Te bond is 2.35 eV \mathring{A}^{-2} , which is much lower than that of In-Te bond (4.33 eV Å⁻²). This quantitatively explains why the Cu-Te bond, rather than the In-Te bond, softens and breaks during the stretching process. In addition, ELF change displayed in Fig. S3† clearly shows that the strong In-Te bonds remain closely connected during the entire tensile process.

3.2.3 Biaxial shear deformation of CuInTe₂. To mimic the nano-indentation experiment, we applied biaxial shear (both shear and compression loads) deformation to understand the underlying failure mechanism of CuInTe2 along the least stress slip system (221)[11-1]. Fig. 4(a) shows the computed shearstress-shear-strain relation as well as the comparison with pure shear deformation. Before 0.142 shear strain, biaxial shearing and pure shearing lead to the same shear stress response. On further increasing shear strain, the shear stress under biaxial shear load was found to be much lower than that under pure shear load. Maximum shear stress of the biaxial shear system is 1.96 GPa at 0.258 shear strain, which is much lower than that (2.43 GPa) of the pure shear system. Beyond maximum stress, the structure rapidly softens and collapses under biaxial shear load, giving rise to a sudden drop in shear stress, which is different from the 'yielding' process under pure shear load. This suggests that compression plays an essential role in determining mechanical strength and deformation mechanism of a biaxial shear system. Fig. 4(b)-(d) display the atomic configurations before and at failure strain and typical bond changes for biaxial shear deformation. At 0.346 shear strain, the Cu-Te and In-Te hexagonal frameworks are compacted resisting external shear and compressive deformation (Fig. 4(b)). At 0.357 shear strain, In1-Te1 bond breaks and hexagonal frameworks change to rectangular (Fig. 4(c)), suggesting that compression leads to structural buckling failure and stress relaxation. The In1-Te1 and Cu1-Te2 bonds shrink, resisting deformation until

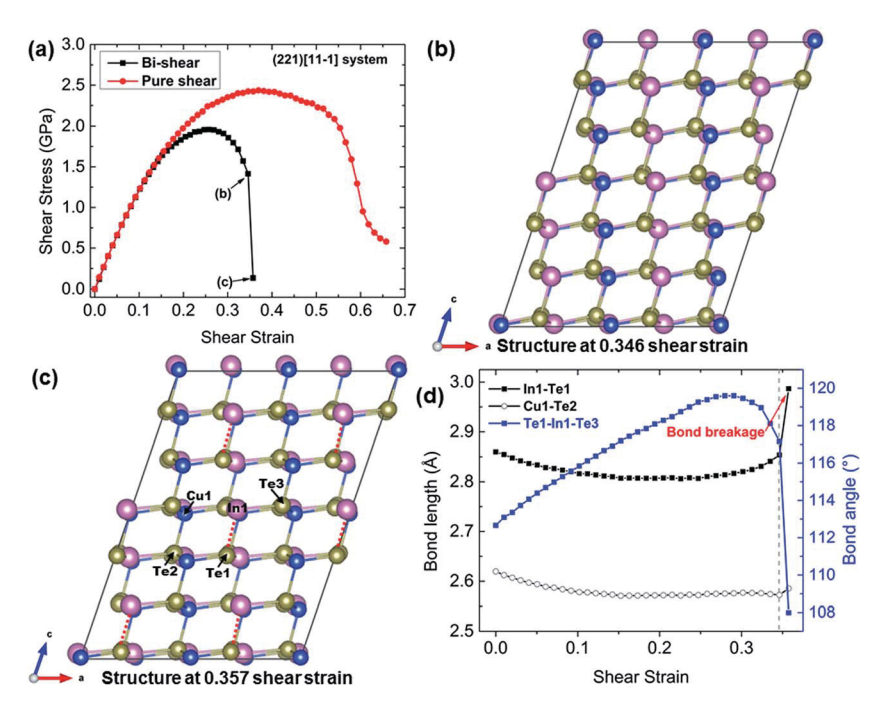


Fig. 4 Biaxial shear deformation of $CuInTe_2$ along the least stress slip system (221)[11–1]. (a) The shear-stress–shear-strain relationship and comparison with that of pure shear deformation. (b) Atomic structure at 0.346 shear strain before failure and (c) atomic structure at failure strain of 0.357. (d) Typical bond lengths (In1–Te1 and Cu1–Te2) and bond angle (Te1–In1–Te3) against shear strain.

maximum shear stress at 0.258 shear strain, as shown in Fig. 4(d), indicating that these bonds have the strongest stiffness. As shear strain increases to 0.346, the In1–Te1 bond starts to stretch, indicating that the structure starts to soften, leading to decreased shear stress, as shown in Fig. 4(a). At the failure strain of 0.357, the sudden increase in bond length represents breakage of In1–Te1 bond, releasing the shear stress. ELF changes, as shown in Fig. S4,† indicate that the In1–Te1 bond along the c axis has no shared electron-pair at failure strain of 0.357, confirming the non-bonding interaction between In1–Te1. Moreover, the Te1–In1–Te3 bond angle drastically drops from 117° to 108°, indicating that the framework shape changes from hexagon to rectangle, as shown in Fig. 4(b) and (c).

3.3 Elastic properties and fracture toughness of CuInTe₂

To provide basic understanding of the stability of CuInTe₂, we computed the elastic matrix (C_{ij}), and then used the Voigt–Reuss–Hill method²⁹ to estimate various elastic properties such as Young's moduli, bulk modulus, shear modulus, and Poisson ratio. Furthermore, we compared these results with previous *ab initio* results using PBE, as listed in Table 1. It is shown that U

correction on Cu 3d electrons has minor effect on the elastic properties of CuInTe₂. Shear modulus is 21.4 GPa, which is much lower than the Young's modulus of 54.2 GPa, indicating that CuInTe₂ is much weaker in resisting shearing compared with tension. This effectively explains why the ideal shear strength (2.43 GPa) of CuInTe₂ is much lower than the ideal tension strength (4.88 GPa). The predicted elastic properties (B, G, E) of CuInTe₂ are much lower than those of the other important TE material TiNiSn (B = 128.8 GPa, G = 67.2 GPa, E = 171.7 GPa) with similar zinc-blende structure. This explains that CuInTe₂ has much lower ideal shear strength (2.43 GPa) than TiNiSn (10.52 GPa).³¹

Similar to elastic modulus (B, G, E), fracture toughness (K_c) is also an important mechanical property for many engineering applications. Our previous studies have indicated that fracture toughness can be successfully estimated from ideal stress-strain relations. ^{32,33} Using the same method, we predicted the fracture toughness of mode I (K_{IC}) , mode II (K_{IIC}) , and mode III (K_{IIIC}) of CuInTe₂, as listed in Table 1. To date, no experimental K_{IC} of CuInTe₂ is reported. However, our previously predicted K_{IC} of PbTe agrees well with the experimental value. ³² We believe that the predicted fracture toughness of CuInTe₂ is correct.

Table 1 Predicted elastic constants (C_{ij}) , bulk modulus (B), shear modulus (G), Young's modulus (E), Poisson ratio (v), fracture toughness (K_{IIc}, K_{IIIc}) of CuInTe₂, and comparison with previous *ab initio* results using PBE. Units of elastic properties and fracture toughness are GPa and MPa m^{1/2}

Method	C_{11}	C_{12}	C_{13}	C_{33}	C_{44}	C_{66}	В	G	E	ν	$K_{\rm Ic}$	K_{IIc}	$K_{ m IIIc}$
$PBE + U$ PBE^{30}	54.7 61.0	31.4 36.9	30.9 40.5	55.0 67.3	26.0 27.2	25.7 24.8	39.0 47	21.4 19	54.2 51	0.27 0.32	0.19	0.37	0.33

Compared with TE oxides, the fracture toughness ($K_{\rm IIc}=0.37~{\rm MPa~m^{1/2}}$, $K_{\rm IIIc}=0.33~{\rm MPa~m^{1/2}}$) of CuInTe₂ is much lower than those of 3D ZnO ($K_{\rm IIc}=0.42~{\rm MPa~m^{1/2}}$, $K_{\rm IIIc}=0.34~{\rm MPa~m^{1/2}}$) and SrTiO₃ ($K_{\rm IIc}=0.58~{\rm MPa~m^{1/2}}$, $K_{\rm IIIc}=0.50~{\rm MPa~m^{1/2}}$), but much higher than those of 2D BiCuSeO ($K_{\rm IIc}=0.26~{\rm MPa~m^{1/2}}$), but much higher than those of 2D BiCuSeO ($K_{\rm IIc}=0.26~{\rm MPa~m^{1/2}}$), $K_{\rm IIIc}=0.21~{\rm MPa~m^{1/2}}$) and NaCo₂O₄ ($K_{\rm IIc}=0.13~{\rm MPa~m^{1/2}}$, $K_{\rm IIIc}=0.11~{\rm MPa~m^{1/2}}$), $K_{\rm III$

3.4 Ideal shear strength of important TE materials

Ideal strength, defined as the first maximum stress at which flawless crystals become mechanically unstable, is a fundamental mechanical characteristic of materials. Herein, we compared the ideal shear strength of CuInTe2 with other important high-performance TE materials, as shown in Fig. 5. In 2D layered TE compounds (Bi₂Te₃, SnSe, Mg₃Sb₂, CaMg₂Sb₂, and CaZn₂Sb₂), Bi₂Te₃ and SnSe have the lowest ideal shear strengths of 0.19 GPa and 0.59 GPa, respectively, because weak van der Waals-like Bi-Te and Sn-Se bonds dominate the deformation of Bi2Te3 and SnSe.21,34 Due to the relatively stronger ionic bonding in 2D Zintl compounds, Mg₃Sb₂, CaMg₂Sb₂, and CaZn₂Sb₂ show higher ideal shear strengths than 2D Bi₂Te₃ and SnSe. 34,36 In 3D TE compounds, TiNiSn and CoSb₃ have the highest ideal shear strengths of 10.52 GPa and 7.17 GPa, respectively, because of the strong 3D Ni-Sn and Co-Sb covalent frameworks in TiNiSn and CoSb₃, respectively.^{23,31} However, lead chalcogenides PbTe, PbSe, and PbS have relatively lower ideal shear strengths of 3.46 GPa, 5.13 GPa, and 7.14 GPa, respectively,32 compared with CoSb3 and TiNiSn, because the 3D Pb-X (X = Te, Se, S) ionic framework is much weaker than the NiSn and Co-Sb covalent framework. CuInTe₂ and InSb have similar tetrahedral In-Te and In-Sb substructures, leading to the same ideal shear strength of 2.43 GPa.22 CuInTe2 has relatively low ideal shear strength among these TE compounds, suggesting that the mechanical

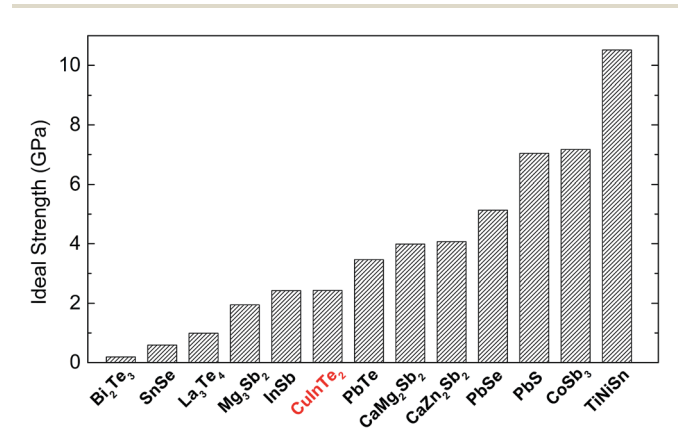


Fig. 5 Computed ideal shear strengths of important TE materials: Bi₂Te₃,²¹ SnSe,³⁴ La₃Te₄,³⁵ Mg₃Sb₂,³⁶ InSb,²² CuInTe₂, PbTe,³² CaMg₂-Sb₂,³⁶ CaZn₂Sb₂,³⁶ PbSe,³² PbS,³² CoSb₃,²³ and TiNiSn.³¹

properties should be enhanced for engineering applications of CuInTe₂.

Conclusions

We applied QM to determine the intrinsic mechanical properties of CuInTe₂, such as ideal shear strength, failure mechanism, and fracture toughness under pure shear, uniaxial tension, and biaxial shear deformations. The major findings are as follows:

- \bullet The lowest ideal shear strength of CuInTe $_2$ is 2.43 GPa along the (221)[11-1] slip system, and the In-Te covalent bond dominates the deformation and shear failure of CuInTe $_2$. This ideal shear strength is relatively low among high-performance TE materials, suggesting its limitation for commercial applications.
- \bullet The lowest ideal tensile strength is 4.88 GPa along the [1–10] tension load, and breakage of the Cu–Te bond leads to tensile failure of CuInTe₂.
- The shear strength is 1.95 GPa under biaxial shear load along the (221)[11–1] slip system. This value is lower than that (2.43 GPa) along its pure shear system. We found that compression shrinks the In–Te bond and leads to buckling of the In–Te hexagonal framework.
- From ideal stress–strain relations of CuInTe₂, we estimated the fracture toughness of mode I ($K_{\rm Ic}=0.19~{\rm MPa~m^{1/2}}$), which is much lower than mode II ($K_{\rm IIc}=0.37~{\rm MPa~m^{1/2}}$) and mode III ($K_{\rm IIIc}=0.33~{\rm MPa~m^{1/2}}$).

Fracture toughness and ideal shear strength of CuInTe₂ are relatively low among important high-performance TE materials, suggesting that improvement of mechanical properties of CuInTe₂ is required for engineering applications.

Conflicts of interest

There are no conflicts to declare

Acknowledgements

This study was partially supported by NSF of China under No. 51772231, the 111 Project of China under Project no. B07040. Q. A. was supported by the National Science Foundation CMMI program under grant no. 1727428. S. M. was thankful for the support by Act 211 Government of the Russian Federation, under No. 02.A03.21.0011 and by the Supercomputer Simulation Laboratory of South Ural State University.³⁷

References

- 1 C. Chang, M. Wu, D. He, Y. Pei, C.-F. Wu, X. Wu, H. Yu, F. Zhu, K. Wang, Y. Chen, L. Huang, J.-F. Li, J. He and L.-D. Zhao, 3D charge and 2D phonon transports leading to high out-of-plane *ZT* in n-type SnSe crystals, *Science*, 2018, **360**(6390), 778–783.
- 2 J. He and T. M. Tritt, Advances in Thermoelectric Materials Research: Looking Back and Moving Forward, *Science*, 2017, 357, 1369.

Paper

- 3 Y. Pei, X. Shi, A. LaLonde, H. Wang, L. Chen and G. J. Snyder, Convergence of Electronic Bands for High Performance Bulk Thermoelectrics, Nature, 2011, 473, 66-69.
- 4 Y. L. Tang, Z. M. Gibbs, L. A. Agapito, G. Li, H. S. Kim, M. B. Nardelli, S. Curtarolo and G. J. Snyder, Convergence of Multi-Valley Bands as the Electronic Origin of High Thermoelectric Performance in CoSb₃ Skutterudites, Nat. Mater., 2015, 14, 1223-1228.
- 5 L. D. Zhao, S. H. Lo, Y. Zhang, H. Sun, G. Tan, C. Uher, C. Wolverton, V. P. Dravid and M. G. Kanatzidis, Ultralow Thermal Conductivity and High Thermoelectric Figure of Merit in SnSe Crystals, Nature, 2014, 508, 373-377.
- 6 S. I. Kim, K. H. Lee, H. A. Mun, H. S. Kim, S. W. Hwang, J. W. Roh, D. J. Yang, W. H. Shin, X. S. Li, Y. H. Lee, G. J. Snyder and S. W. Kim, Dense Dislocation Arrays Embedded in Grain Boundaries for High-Performance Bulk Thermoelectrics, Science, 2015, 348, 109-114.
- 7 M. T. Barako, W. Park, A. M. Marconnet, M. Asheghi and K. E. Goodson, Thermal Cycling, Mechanical Degradation, and the Effective Figure of Merit of a Thermoelectric Module, J. Electron. Mater., 2013, 42, 372–381.
- 8 R. H. Liu, L. L. Xi, H. L. Liu, X. Shi, W. Q. Zhang and L. D. Chen, Ternary compound CuInTe2: a promising thermoelectric material with diamond-like structure, Chem. Commun., 2012, 48(32), 3818-3820.
- 9 G. Zhou and D. Wang, High thermoelectric performance from optimization of hole-doped CuInTe2, Phys. Chem. Chem. Phys., 2016, 18(8), 5925-5931.
- 10 N. Cheng, R. Liu, S. Bai, X. Shi and L. Chen, Enhanced thermoelectric performance in Cd doped CuInTe2 compounds, J. Appl. Phys., 2014, 115(16), 163705.
- 11 W. Liu, X. J. Tan, K. Yin, H. J. Liu, X. F. Tang, J. Shi, Q. J. Zhang and C. Uher, Convergence of Conduction Bands as a Means of Enhancing Thermoelectric Performance of n-Type Mg2Si1-xSnx Solid Solutions, Phys. Rev. Lett., 2012, 108(16), 166601.
- 12 B. Duan, J. Yang, J. R. Salvador, Y. He, B. Zhao, S. Y. Wang, P. Wei, F. S. Ohuchi, W. Q. Zhang, R. P. Hermann, O. Gourdon, S. X. Mao, Y. W. Cheng, C. M. Wang, J. Liu, P. C. Zhai, X. F. Tang, Q. J. Zhang and J. H. Yang, Electronegative guests in CoSb3, Energy Environ. Sci., 2016, 9(6), 2090-2098.
- 13 H. J. Chen, C. Y. Yang, H. L. Liu, G. H. Zhang, D. Y. Wan and F. Q. Huang, Thermoelectric properties of CuInTe2/ graphene composites, CrystEngComm, 2013, 15(34), 6648-
- 14 Y. B. Luo, J. Y. Yang, Q. H. Jiang, W. X. Li, D. Zhang, Z. W. Zhou, Y. D. Cheng, Y. Y. Ren and X. He, Progressive Regulation of Electrical and Thermal Transport Properties to High-Performance CuInTe2 Thermoelectric Materials, Adv. Energy Mater., 2016, 6(12), 1600007.
- 15 J. F. Yang, S. P. Chen, Z. L. Du, X. L. Liu and J. L. Cui, Lattice defects and thermoelectric properties: the case of p-type CuInTe2 chalcopyrite on introduction of zinc, Dalton Trans., 2014, 43(40), 15228-15236.
- 16 Y. B. Luo, J. Y. Yang, Q. H. Jiang, W. X. Li, Y. Xiao, L. W. Fu, D. Zhang, Z. W. Zhou and Y. D. Cheng, Large enhancement

- of thermoelectric performance of CuInTe2 via a synergistic strategy of point defects and microstructure engineering, Nano Energy, 2015, 18, 37-46.
- 17 G. Kresse and J. Furthmuller, Efficiency of ab initio Total Energy Calculations for Metals and Semiconductors Using a Plane-Wave Basis Set, Comput. Mater. Sci., 1996, 6, 15-50.
- 18 G. Kresse and J. Furthmuller, Efficient Iterative Schemes for ab initio Total-Energy Calculations Using a Plane-Wave Basis Set, Phys. Rev. B, 1996, 54, 11169-11186.
- 19 G. Kresse and D. Joubert, From Ultrasoft Pseudopotentials to the Projector Augmented-Wave Method, Phys. Rev. B, 1999,
- 20 J. Perdew, K. Burke and M. Ernzerhof, Generalized Gradient Approximation Made Simple, Phys. Rev. Lett., 1996, 77, 3865-3868.
- 21 G. Li, U. Aydemir, S. I. Morozov, M. Wood, Q. An, P. C. Zhai, Q. J. Zhang, W. A. Goddard and G. J. Snyder, Superstrengthening Bi₂Te₃ through Nanotwinning, Phys. Rev. Lett., 2017, 119(8), 085501.
- 22 G. Li, S. I. Morozov, Q. Zhang, Q. An, P. Zhai and G. J. Snyder, Enhanced Strength Through Nanotwinning in the Thermoelectric Semiconductor InSb, Phys. Rev. Lett., 2017, **119**(21), 215503.
- 23 G. Li, Q. An, W. Li, W. A. Goddard, P. Zhai, Q. Zhang and G. J. Snyder, Brittle Failure Mechanism in Thermoelectric Skutterudite CoSb3, Chem. Mater., 2015, 27(18), 6329-6336.
- 24 B. Silvi and A. Savin, Classification of Chemical Bonds Based on Topological Analysis of Electron Localization Functions, Nature, 1994, 371, 683-686.
- 25 P. Prabukanthan and R. Dhanasekaran, Growth of CuInTe2 Crystals by Iodine Transport and Characterization, Mater. Res. Bull., 2008, 43(8-9), 1996-2004.
- 26 M. de Jong, W. Chen, T. Angsten, A. Jain, R. Notestine, A. Gamst, M. Sluiter, C. Krishna Ande, S. van der Zwaag, J. J. Plata, C. Toher, S. Curtarolo, G. Ceder, K. A. Persson and M. Asta, Charting the Complete Elastic Properties of Inorganic Crystalline Compounds, Sci. data., 2015, 2, 150009.
- 27 S. Ogata, J. Li and S. Yip, Ideal pure shear strength of aluminum and copper, Science, 2002, 298(5594), 807-811.
- 28 A. van de Walle, M. Asta and G. Ceder, The alloy theoretic automated toolkit: A user guide, Calphad, 2002, 26(4), 539-553.
- 29 D. H. Chung, Elastic Moduli of Single-Crystal and Polycrystalline MgO, Philos. Mag., 1963, 8, 833-841.
- 30 S. Sharma, A. S. Verma, R. Bhandari and V. K. Jindal, Ab initio studies of structural, elastic and thermal properties of copper indium dichalcogenides (CuInX2: X = S, Se, Te), Comput. Mater. Sci., 2014, 86, 108-117.
- 31 G. Li, Q. An, U. Aydemir, W. A. Goddard III, M. Wood P. Zhai, Q. Zhang and G. J. Snyder, Enhanced Ideal Strength of Thermoelectric Half-Heusler TiNiSn by Sub-Structure Engineering, J. Mater. Chem. A, 2016, 4, 14625-14636.
- 32 G. Li, U. Aydemir, B. Duan, M. T. Agne, H. Wang, M. Wood, Q. Zhang, P. Zhai, W. A. Goddard III and G. J. Snyder, Microand Macromechanical Properties of Thermoelectric Lead

- Chalcogenides, ACS Appl. Mater. Interfaces, 2017, 9(46), 40488-40496.
- 33 G. Li, U. Aydemir, S. I. Morozov, S. A. Miller, Q. An, W. A. Goddard III, P. Zhai, Q. Zhang and G. J. Snyder, Mechanical Properties in Thermoelectric Oxides: Ideal Strength, Deformation Mechanism, and Fracture Toughness, *Acta Mater.*, 2018, 149, 341–349.
- 34 G. Li, U. Aydemir, M. Wood, W. A. Goddard III, P. Zhai, Q. Zhang and G. J. Snyder, Ideal Strength and Deformation Mechanism in High-Efficiency Thermoelectric SnSe, *Chem. Mater.*, 2017, **29**, 2382–2389.
- 35 G. Li, U. Aydemir, M. Wood, W. A. Goddard III, P. Zhai, Q. Zhang and G. J. Snyder, Mechanical properties of thermoelectric lanthanum telluride from quantum mechanics, *J. Phys. D: Appl. Phys.*, 2017, 50(27), 274002.
- 36 G. Li, U. Aydemir, M. Wood, Q. An, W. A. Goddard Iii, P. Zhai, Q. Zhang and G. J. Snyder, Deformation Mechanisms in High-Efficiency Thermoelectric Layered Zintl Compounds, *J. Mater. Chem. A*, 2017, 5(19), 9050–9059.
- 37 P. S. Kostenetskiy, and A. Y. Safonov, SUSU Supercomputer Resources. Proceedings of the 10th Annual International Scientific Conference on Parallel Computing Technologies, Arkhangelsk, Russia, 2016.